frontiers | Frontiers in Earth Science

TYPE Original Research
PUBLISHED 06 March 2023
DOI 10.3389/feart.2023.1141379

OPEN ACCESS

EDITED BY
Nicola Colombo,
National Research Council (CNR), Italy

REVIEWED BY
Lukasz Stachnik,
University of Wrocław, Poland
Cristian Villarroel,
CONICET Centro de Investigaciones de la Geósfera y Biósfera (CIGEOBIO), Argentina

*CORRESPONDENCE
Ulrike Nickus,
ulrike.nickus@uibk.ac.at

SPECIALTY SECTION
This article was submitted to Hydrosphere, a section of the journal Frontiers in Earth Science

RECEIVED 10 January 2023
ACCEPTED 22 February 2023
PUBLISHED 06 March 2023

CITATION
Nickus U, Thies H, Krainer K, Lang K, Mair V and Tonidandel D (2023), A multi-millennial record of rock glacier ice chemistry (Lazaun, Italy). *Front. Earth Sci.* 11:1141379. doi: 10.3389/feart.2023.1141379

A multi-millennial record of rock glacier ice chemistry (Lazaun, Italy)

Ulrike Nickus[1]*, Hansjörg Thies[2], Karl Krainer[3], Kathrin Lang[4], Volkmar Mair[4] and David Tonidandel[4]

[1]Department of Atmospheric and Cryospheric Sciences, University of Innsbruck, Innsbruck, Austria, [2]Institute of Interdisciplinary Mountain Research, Austrian Academy of Science, Innsbruck, Austria, [3]Department of Geology, University of Innsbruck, Innsbruck, Austria, [4]Office for Geology and Building Materials Testing, Autonomous Province of Bolzano, Bolzano, Italy

Active rock glaciers—known as mixtures of unconsolidated debris with interstitial ice, ice lenses or a core of massive ice—are widespread indicators of mountain permafrost. The age of a frozen rock glacier core in the Central European Alps (Lazaun, Italy) was dated to about 10,000 years. Here we report on the chemical composition of the frozen Lazaun core. The ice containing part of the core extended from about 2.8 m down to 24 m depth and consisted of two lobes—both a mix of ice and debris, separated by more than 3 m thick almost ice-free layer. The two lobes of the core showed layers of high solute content and peak values of electrical conductivity exceeding 1,000 µS/cm, but they differed in acidity and metal concentration. High acidity (minimum pH of 4.15) and high levels of elements like nickel, cobalt, zinc, manganese, iron and aluminum characterized the upper lobe, while neutral to alkaline pH and low metal values prevailed in the bottom lobe. We attributed solutes accumulated in the ice matrix to the weathering of bedrock minerals, with peak values favored by the oxidation of pyrite, or by an enhanced reactive surface area in fine-grained sediment layers. The chemical composition of the ice core also revealed signals of prehistoric atmospheric deposition from different sources including wood combustion, metal ore mining, and large volcanic eruptions (Thera, Aniakchak II). To our knowledge, this is the first study that presents the chemical stratigraphy of an entire rock glacier ice core.

KEYWORDS

alpine permafrost, active rock glacier, ice core, ice chemistry, Lazaun

1 Introduction

Permafrost is an important part of the global cryosphere. About 17% of the global exposed land surface and 25% of the Northern Hemisphere are estimated to be perennially frozen (Biskaborn et al., 2019), either at high latitudes or high altitudes. Impressive features of mountain permafrost are active rock glaciers, i.e., lobate-to tongue-shaped bodies of unconsolidated rocks and debris supersaturated with interstitial ice and ice lenses (Barsch, 1996). Active rock glaciers (ARGs) move downslope or downvalley by creep as a consequence of the deforming internal ice (Haeberli, 1985; Barsch, 1996). ARGs of periglacial origin consist of a core of ice-supersaturated perennially frozen talus covered by a seasonally frozen layer of debris, known as the active layer. The ice of these talus-derived ARGs originates from rain and meltwater, which percolate through the core of rock and debris and freeze at lower depths (Haeberli et al., 2006; Jones et al., 2019). Details on the

internal structure of ARGs have been provided by geophysical methods like ground-penetrating radar, seismic refraction tomography or electrical resistivity tomography (Hausmann et al., 2007; Hauck et al., 2011; Leopold et al., 2011; Hausmann et al., 2012), as well as by core drillings. However, the extraction of ARG cores has yet been confined to a few sites in the European Alps (for instance Reichenkar, Ölgrube and Kaiserberg in Austria, Hohe Gaisl/Croda Rossa, Murfreit/Sella and Foscagno in Italy, Murtel-Corvatsch and Muragl in Switzerland) and in the US (Galena Creek) (Barsch et al., 1979; Haeberli et al., 1998; Steig et al., 1998; Haeberli et al., 1999; Arenson et al., 2002; Guglielmin et al., 2004; Krainer et al., 2015). The ice of individual European ARGs dates back to the Early Holocene. For instance, an age of about 10,300 years has been derived by radiocarbon dating of fossil plant remains for the frozen core of Lazaun rock glacier (Italy) (Krainer et al., 2015). A likely age of several thousand years is given for Murtél-Corvatsch (Switzerland) (Haeberli et al., 1999), while an age of 2,200 years is reported for the relict glacier ice within the permafrost of Foscagno rock glacier (Italy) (Guglielmin et al., 2004).

The chemistry of rock glacier ice is expected to reveal impacts of bedrock weathering and of atmospheric deposition, but there is still a major lack of knowledge on the solute content of rock glacier ice due to the limited number of extracted cores (Guglielmin et al., 2004). Increased substance contents in high elevation surface waters downstream of rock glaciers (Williams et al., 2006; Thies et al., 2007; Williams et al., 2007; Thies et al., 2013; Ilyashuk et al., 2014; Fegel et al., 2016; Colombo et al., 2018a; Colombo et al., 2018b; Thies et al., 2018; Colombo et al., 2019; Jones et al., 2019) point to a temporary contribution of highly concentrated meltwater from the ice matrix of rock glaciers in late summer, and provide an indirect evidence of the solutes accumulated in the ice of ARGs. In view of increasing air temperatures due to climate warming, an enhanced degradation of rock glacier ice and thus a higher fraction of meltwater to the outflows of ARGs is hypothesised (Jones et al., 2019) with potential impacts on freshwater ecosystems downstream of ARGs (Brighenti et al., 2019a; Brighenti et al., 2019b; Colombo et al., 2020; Peszek et al., 2022).

In this study, we investigate the chemical stratigraphy of a frozen rock glacier core, extracted in the Central Eastern Alps (Lazaun, Italy). We discuss processes that potentially had an impact on vertical solute profiles in the ice matrix of the core. According to our knowledge, this is the first study that presents the chemistry of an entire rock glacier ice core.

2 Study site and methods

Lazaun rock glacier (LZRG) is located at 46°44′49″N and 10°45′20″E in the Schnals Valley in the southern Ötztal Alps (Northern Italy) (Figure 1). The active tongue-shaped rock glacier extends from 2,480 to 2,700 m above sea level in a north-east facing cirque and covers a horizontal surface area of 0.12 km^2. Debris is supplied from frost weathering of a ridge south of LZRG. The bedrock in the catchment of LZRG is composed of polymetamorphic rocks of the Ötztal-Stubai Metamorphic Complex of the austroalpine Ötztal-Bundschuh Nappe System that is mainly composed of paragneiss and mica schists, orthogneiss and amphibolite (Hoinkes and Thöni 1993; Hoinkes et al., 2021). The main bedrock types at Lazaun are paragneiss (biotite-plagioclase gneiss) and micaschist. Orthogneiss is rare and amphibolite is absent (Bressan, 2007). Carbonate rocks do not occur. LZRG is composed of debris derived from these bedrock types, mainly paragneiss and mica schist. Paragneiss (biotite-plagioclase gneiss) is composed of quartz, plagioclase, biotite, garnet, muscovite, chlorite, staurolite, some chlorite and accessory minerals such as tourmaline, titanite and opaque grains (ilmenite, sulfide minerals like pyrite, chalkopyrite, and pyrrhotine). Mica schists have a similar mineralogical composition of quartz, plagioclase, muscovite, biotite, chlorite, garnet, staurolite, rare kyanite and accessory minerals including zircon, tourmaline, titanite, and opaque minerals. Orthogneiss is fine-grained and composed of quartz, feldspars, biotite, muscovite, garnet, accessory opaque minerals and locally some chlorite and carbonate minerals. More information on LZRG (regarding geomorphology, flow velocities, borehole temperature profiles, core stratigraphy, radiocarbon core dating, etc.,) is given by Krainer et al. (2015).

The vertical LZRG core of 12.5 cm diameter was extracted from the lower part of LZRG in summer 2010 using a cooled core drilling device (Nenzi Gelmina by Landservice Srl, Italy). The core was extracted at a distance of about 240 m from the rock glacier front at an elevation of 2,580 m and covered a length of 40 m. The ice-containing parts of the core were put into cooling boxes at the field site, and were stored at a temperature of −20°C prior to chemical analysis. Sub-samples of the frozen core were taken at 10–55 cm intervals for the determination of the ice content, for chemical analysis, and for radiocarbon dating resulting in a total of 149 samples (Krainer et al., 2015). Prior to chemical analysis, the mixture of ice and debris was melted at room temperature in closed containers and filtered through 0.45 µm mesh filters (ME 25, Schleicher and Schuell). Water samples were then analysed for pH, conductivity, major ions and metals. Polyethylene bottles used for further analysis were all pre-cleaned according to standard procedures (for ion analysis bottles were rinsed with diluted HCl and then soaked and rinsed with ultrapure water; for element analysis bottles were pre-cleaned with 3% HNO_3 and samples were acidified with HNO_3 (Merck 65% suprapur) to about 1 (wt) %). Specific electrical conductivity (at 25°C) was measured with a WTW LF-92 m, and pH was determined with a WTW pH-91 m and a Hamilton flushtrode. Ion concentrations were analysed by ion exchange chromatography (Dionex DX-500 and ICS-1000) applying suppressed conductivity detection. Major anions and cations were separated with AS11 and CS12A analytical columns and injection volume was 20 µl. Individual stock solutions of 1,000 mg/kg (Merck CertiPur) were diluted for mixed standard solutions. Analytical accuracy was less than 1.5% and precision was less than 3% for all ions. Method detection limits (MDL) were between 0.04 and 0.09 mg/L for all ions. An Inductively Coupled Plasma Optical Emission Spectrometer ICP OES (Horiba Jobin Yvon Activa) was used for elemental metal analysis. Merck CertiPur ICP multi-element stock solutions and AlfaAesar single element ICP stock solutions were used for standard solutions and certified reference solutions from Environment Canada (trace element fortified materials TM-15.2, TMDA-61.2, and TMDA-70) were applied for quality control. Deviation of measured values generally ranged below 10% of certified concentrations. Detection limits were 3 µg/L for Al, Ba, Co, Cu, Mn, Ni, Sr, and

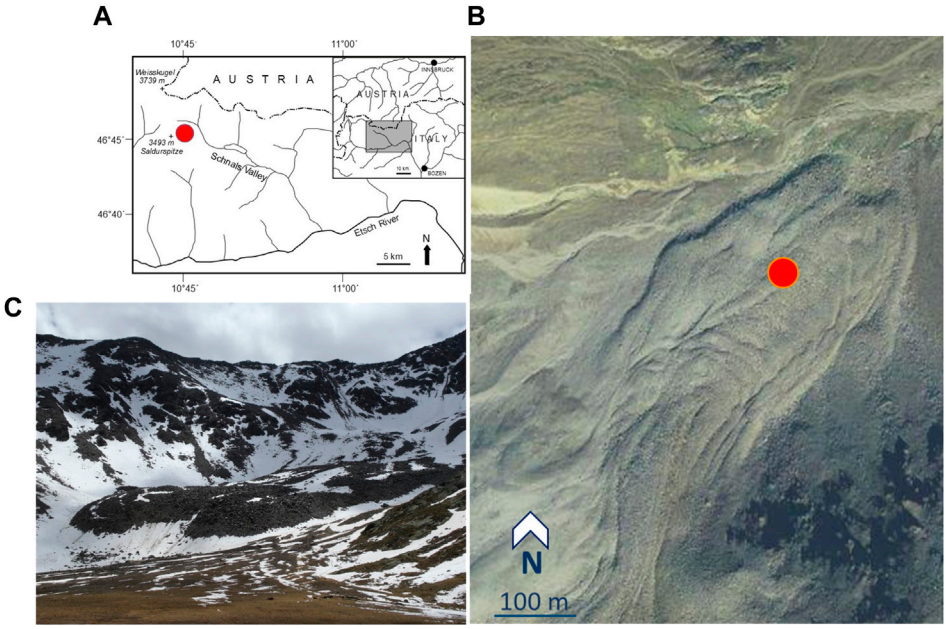

FIGURE 1
The active rock glacier Lazaun (Northern Italy). **(A)** Location of the rock glacier, close to the border Italy—Austria, indicated by the red dot. **(B)** Location of the site at Lazaun rock glacier where the core was drilled (red dot). Orthophoto by terraitaly products TM—© C.G.R. S.P.A—PARMA. **(C)** Tongue and lower part of Lazaun rock glacier (Photo by K. Krainer).

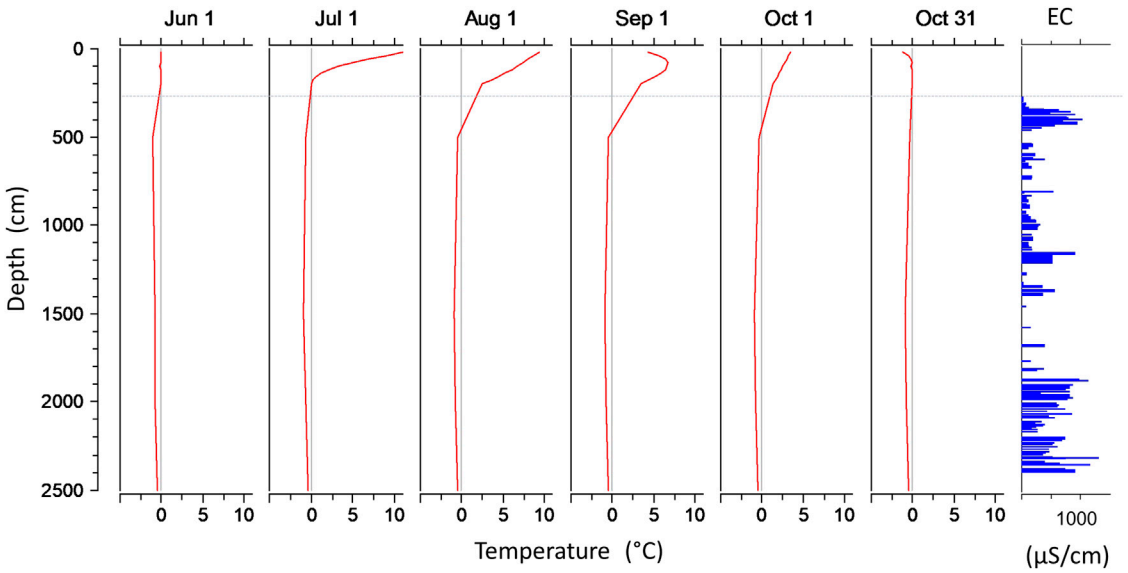

FIGURE 2
Vertical profiles of daily average temperature in the LZRG core for selected days during summer 2012 and profile of electrical conductivity (µS/cm). Horizontal dashed line indicates the upper limit of the frozen core.

Zn, and 10 µg/L for Fe and Si (Thies et al., 2007; Thies et al., 2013; Thies et al., 2018). Alkalinity was determined by Gran titration in case there was enough water left for analysis. Temperature in the drill hole of the LZRG core was measured at several levels (i.e., every 0.2 m down to 2 m depth, and every 5 m between 5 and 40 m depth) by a thermistor chain (YSI 4403110 10 k Ohm, accuracy of 0.1°C) and data are available at hourly intervals for the period June to October 2012. Statistica 13 software was used for statistical analysis.

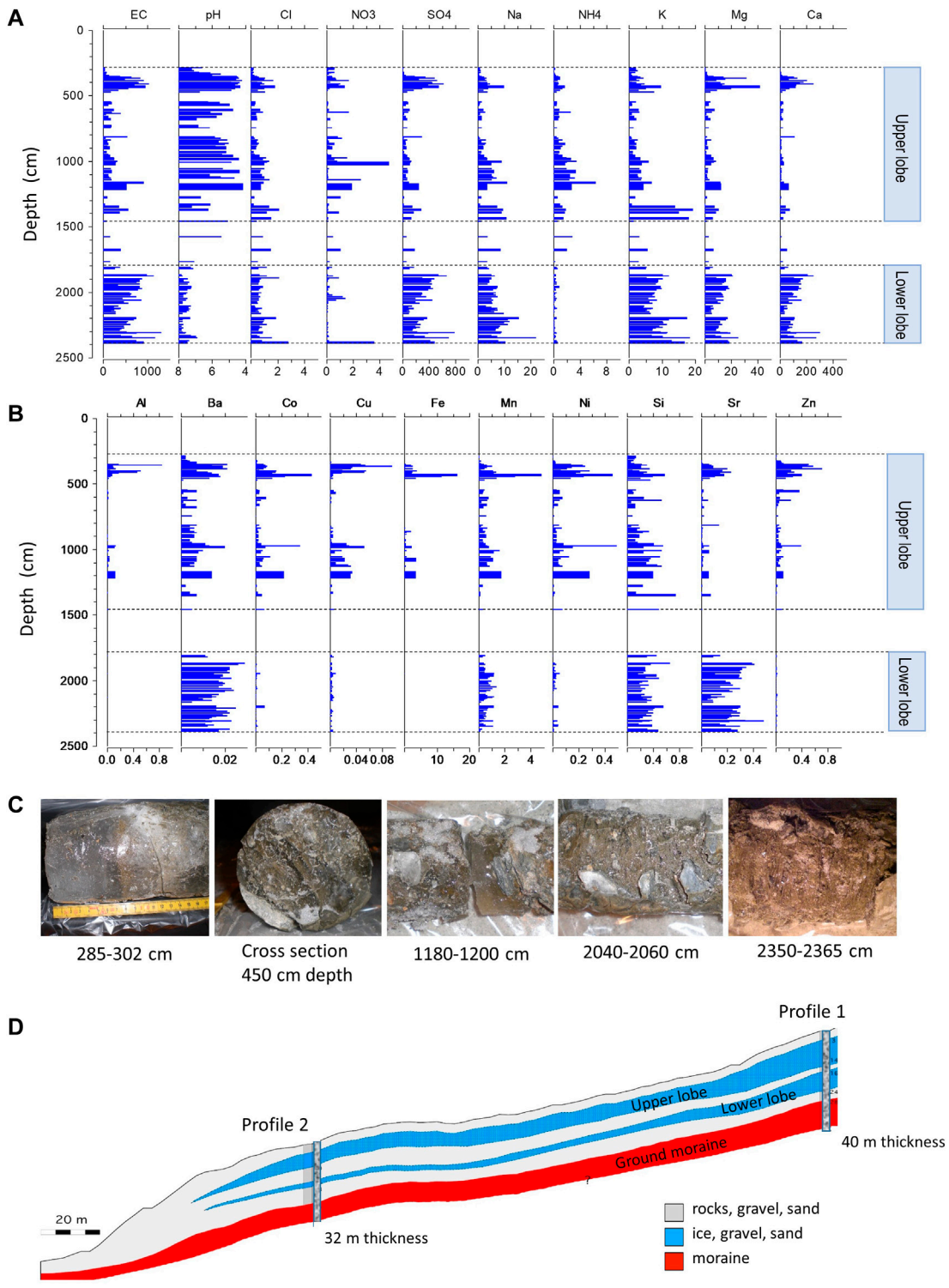

FIGURE 3
Chemical stratigraphy of the Lazaun rock glacier core. **(A)** Vertical profiles of electrical conductivity (EC) in µS/cm, major ions (chloride, nitrate, sulfate, sodium, ammonium, potassium, magnesium, calcium) in mg/L and pH (the scale is from the right pH 4 to the left pH 8). **(B)** Vertical profiles of selected metals in mg/L. The depth range of both upper and lower lobe are indicated in **(A, B)**. **(C)** Different segments of the LZRG core (Photos by H. Thies). **(D)** Schematic of the structure of LZRG derived from two vertical drillings (Profile one is the LZRG core as discussed here, Profile two is a 32 m long core close to the front of the rock glacier—for more detailed information see Krainer et al., 2015).

3 Results

The 40 m long vertical LZRG core can be divided into several segments. The active layer without any ice covered the top 2.8 m. It was followed by the frozen part of the core down to a depth of 25 m. The frozen core consisted of two active lobes, both a mixture of ice and debris. An almost ice-free layer between 14.7 and 18.1 m depth separated the two lobes. No ice was found below 25 m down to 40 m, the lower end of the LZRG core (Figure 3D). The temperature profile measured in the borehole between June and October 2012 nicely reflected the extent of the active layer. Down to a depth of 2 m, daily temperature means were positive from June through October, while values remained ≤0°C between 5 and 35 m (Figure 2).

Radiocarbon dating of plant microfossils revealed a total age of about 10,300 cal yr BP for the LZRG core down to 25 m depth (Krainer et al., 2015). The first ice at 2.8 m depth corresponded to an age of ~2,200 years according to the age-depth model. The upper lobe covered a time span from 2,200 to 3,900 cal·yr BP, while the lower lobe was dated to the period from ~5,300 to 10,300 cal·yr BP. The almost ice-free part of the core in between the two lobes was interpreted as a more than 500-year long drought period with ice melting and the formation of ice-free debris layers (Krainer et al., 2015). The oldest chemically analysed ice was dated to about 9,400 cal·yr BP (as the 24–25 m layer contained too little ice for chemical analysis).

Here we focus on the chemical stratigraphy of the frozen LZRG core. We present the vertical distribution of major ions and metals along the core profile and discuss differences in the overall chemical characteristics of the ice in the two lobes. The vertical distribution of analysed ions and elements in the ice matrix of the LZRG core is given in Figure 3.

3.1 Chemistry of the upper lobe

The upper lobe of LZRG extended from 2.8 to 14.7 m. The ice matrix was acidic with a median pH of 5.38 and a minimum pH of 4.15. Electrical conductivity (EC) revealed a high variability along the vertical profile with a median value of 174 µS/cm and a maximum EC of >1,000 µS/cm (Table 1; Figure 3). The total amount of dissolved ions was dominated by sulfate, calcium, and magnesium. Generally, these three ions comprised ≥90% of the ion

TABLE 1 Median, minimum and maximum values of electrical conductivity EC, major ions and pH in different depth intervals of the LZRG core as well as number of samples (n). EC given in µS/cm, all ions in mg/L.

Depth		EC	Cl	NO_3	SO_4	Na	NH_4	K	Mg	Ca	pH
285–480 cm											
	Median	439	0.6	0.4	219	2.3	0.6	2.7	7.7	64	4.74
	Min	39	0.1	0.0	9.1	0.4	0.03	0.5	0.7	3.7	4.22
	Max	1029	1.8	1.7	620	10	1.7	9.8	42	252	7.19
	n	20	20	20	20	20	20	20	20	20	20
545–1470 cm											
	Median	169	0.6	0.2	69	2.7	1.4	2.4	3.1	14	5.44
	Min	41	0.2	0.0	14	0.4	0.4	0.7	0.5	4.1	4.15
	Max	918	2.1	4.7	288	11	6.4	19	12	110	7.18
	n	43	42	42	42	42	42	42	42	42	36
285–1470 cm											
Upper lobe											
	Median	174	0.6	0.2	72	2.6	1.0	2.5	3.3	18	5.38
	Min	39	0.1	0.0	9.1	0.4	0.03	0.5	0.5	3.7	4.15
	Max	1029	2.1	4.7	620	11	6.4	19	42	252	7.19
	n	63	62	62	62	62	62	62	62	62	56
1810–2400 cm											
Lower lobe											
	Median	603	0.7	0.1	269	7	0.3	8	12	93	7.48
	Min	175	0.3	0.01	63	2.3	0.1	4	3	20	6.12
	Max	1313	2.8	4	784	22	0.9	19	25	300	7.82
	n	45	46	46	46	46	46	46	46	46	44

TABLE 2 Median, minimum and maximum values of metal concentrations in different depth intervals of the LZRG core as well as number of samples (n). All concentrations are given in mg/L (LOD: limit of detection).

Depth		Al	Ba	Co	Cu	Fe	Mn	Ni	Si	Sr	Zn
285–480 cm											
	Median	0.052	0.010	0.062	0.004	0.392	0.441	0.124	0.208	0.073	0.203
	Min	<LOD	0.001	<LOD	<LOD	<LOD	0.016	<LOD	0.025	0.002	<LOD
	Max	0.842	0.021	0.430	0.095	16.2	4.8	0.460	0.579	0.232	0.705
	n	20	20	20	20	20	20	20	20	20	20
545–1470 cm											
	Median	0.006	0.006	0.032	0.004	0.019	0.537	0.047	0.240	0.014	0.057
	Min	<LOD	0.001	0.005	<LOD	<LOD	0.111	0.007	0.063	0.004	0.009
	Max	0.129	0.020	0.339	0.052	3.7	1.7	0.490	0.746	0.139	0.391
	n	36	36	36	36	36	36	36	36	36	36
285–1470 cm											
Upper lobe											
	Median	0.008	0.007	0.034	0.004	0.035	0.494	0.053	0.217	0.014	0.068
	Min	<LOD	0.001	<LOD	<LOD	<LOD	0.016	<LOD	0.025	0.002	<LOD
	Max	0.842	0.021	0.430	0.095	16.2	4.8	0.490	0.746	0.232	0.705
	n	56	56	56	56	56	56	56	56	56	56
1810–2400 cm											
Lower lobe											
	Median	<LOD	0.017	0.004	0.003	<LOD	0.536	0.007	0.302	0.233	0.011
	Min	<LOD	0.005	<LOD	<LOD	<LOD	0.153	<LOD	0.166	0.050	0.003
	Max	0.009	0.029	0.069	0.009	0.169	1.4	0.054	0.655	0.479	0.030
	n	46	46	46	46	46	46	46	46	46	46

sum. Median concentrations were 72 mg/L for sulfate, 18 mg/L for calcium and 3 mg/L for magnesium, and maxima exceeded median values by about one order of magnitude. Median metal concentrations were generally in the µg/L range and showed a high vertical variability along the core profile. Minima of metal concentrations were close to or below the limits of detection and maxima between one and two orders of magnitude higher than median concentrations (Table 2).

A specific section of high ion and elemental concentrations was found between 3.4 and 4.8 m depth (Figure 3). There, acidity was high with a median pH of 4.74 and concentrations of sulfate, calcium, magnesium and EC exceeded median values of the entire lobe by a factor of two to four. A similar behavior was found for the median concentrations of aluminum, cobalt, iron, nickel, strontium, and zinc, all of which were two times (nickel) to 10 times (iron) higher than the corresponding median values of the entire upper lobe (Tables 1, 2). However, above this core section of high acidity, high EC, ion and metal contents, we found about 60 cm ice of low substance concentrations and neutral pH values (Figure 3). This layer between 2.85 and 3.4 m depth (i.e., the top 60 cm of the frozen LZRG core with maximum ice fractions of 92%–98% vol) experienced positive temperatures during summer months (Figure 2).

3.2 Chemistry of the lower lobe

In the ice matrix of the lower lobe (i.e., at 18.1–24 m depth), neutral to slightly alkaline pH values prevailed with a median of pH 7.48 and combined with high values of alkalinity (median alkalinity of 632 µeq/L) and EC (median EC of 603 µS/cm). The absolute peak EC of the frozen LZRG core was >1,300 µS/cm in the lowest meter of the core (Table 1; Figure 3). Ion load was determined by sulfate, calcium and magnesium, similar to the upper lobe of the LZRG core. Median concentrations were 269 mg/L (sulfate), 93 mg/L (calcium) and 12 mg/L (magnesium) and maxima exceeded median values by a factor of two to three. Median concentrations of the metals aluminum, cobalt, copper, iron, nickel, and zinc were in the range of a few µg/L, but values of these elements were close to or below the limits of detection in several layers of the lower lobe (Table 2; Figure 3). Barium, manganese and silica were in the same concentration range as in the upper lobe, while median strontium

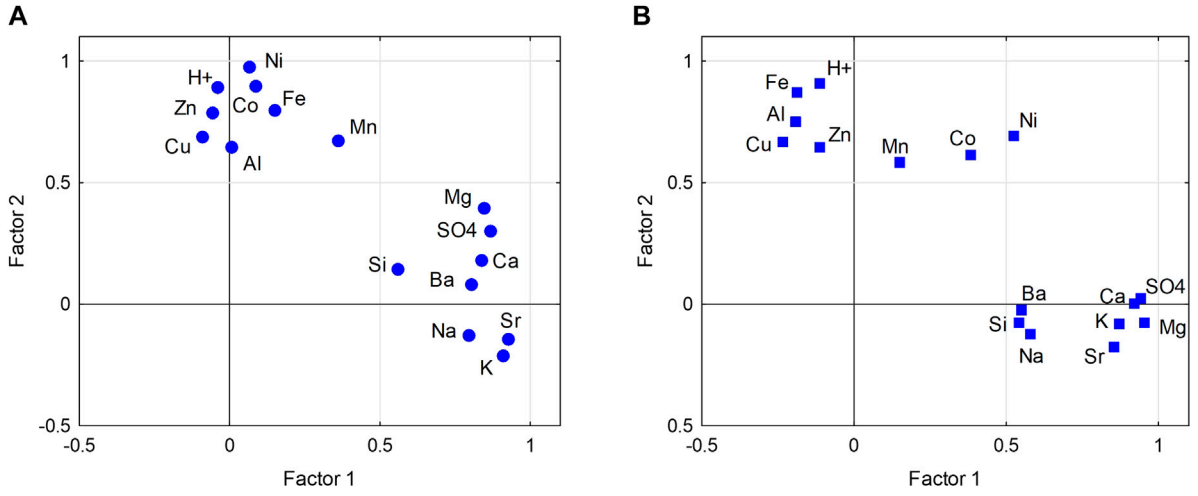

FIGURE 4
Factor analysis biplots (varimax rotated) showing the variable loadings: **(A)** Upper lobe, **(B)** lower lobe of the LZRG core.

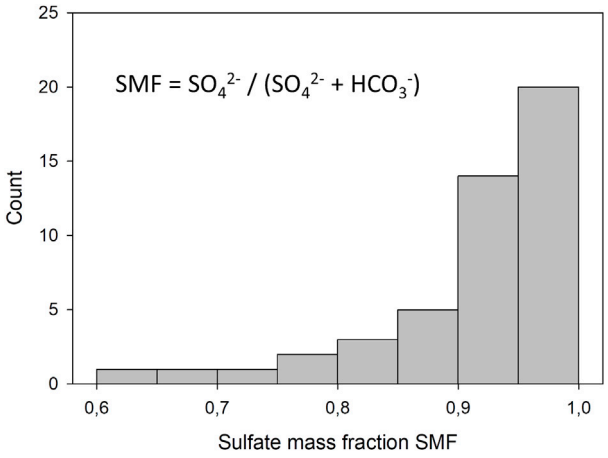

FIGURE 5
Histogram of the sulfate mass fraction (SMF) in samples of the LZRG core.

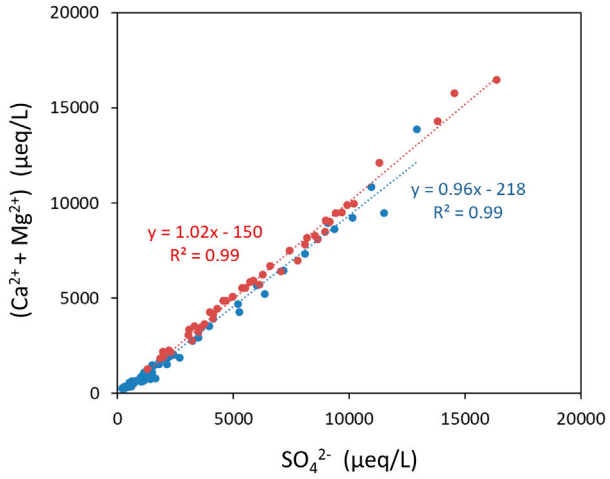

FIGURE 6
Scatterplot of sulfate vs. (calcium + magnesium) in µeq/L for LZRG samples. Values of the upper lobe in blue, values of the lower lobe in red.

concentration exceeded the median of the upper lobe by more than one order of magnitude.

3.3 Linkage of chemical variables

Spearman rank correlation was applied to ions and elements analyzed in the LZRG ice core (Supplementary Table S1). In the upper lobe, most correlations are significant at $p < 0.01$. We found a strong positive correlation between acidity and metals like nickel, iron, copper, cobalt, aluminum, zinc, and manganese (r = 0.7–0.87) and there was a strong correlation among most of these metals. Correlation was also strongly positive between calcium, magnesium, strontium, and sulfate (r = 0.9–0.97), and between silica, sodium and potassium (r ~ 0.8). Contrary to the upper lobe of the LZRG core, less significant correlations among ions and elements were found in the lower lobe (Supplementary Table S1). Both iron and aluminum were excluded from correlation analysis due to their very low concentrations (partly <LOD). The only strong positive correlation was between calcium, magnesium, strontium, potassium and sulfate (r = 0.79–1.0), while correlations between acidity and metals were low and limited to nickel, cobalt and zinc (r = 0.4–0.5).

Factor analysis was applied to explore potential controls on the concentration of ions and metals in the ice of the LZRG core. We used principal component analysis for factor extraction and Varimax rotation. A two-factor solution explained ~70% of the total variance in the upper lobe and 62% in the lower lobe (Supplementary Table S2). Sulfate, potassium, magnesium,

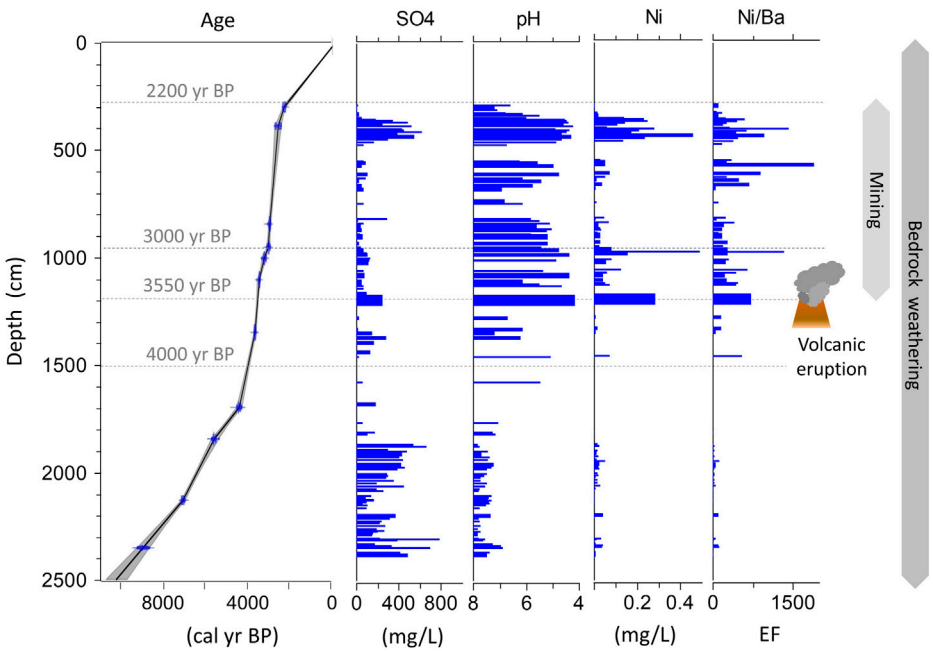

FIGURE 7
Schematics indicating the timeframe of factors that are considered to impact on the chemical composition of the LZRG core combining the age-depth model of the LZRG core (in yr cal BP) adapted from (Krainer et al., 2015) and vertical profiles of sulfate (mg/L), pH (reversed scale right to left), nickel (mg/L) and the enrichment factor (EF) of nickel (with barium as crustal tracer).

calcium and strontium loaded strongly (loading >0.7) on factor 1 in both lobes, barium and sodium only in the upper lobe. This factor is considered to describe the impact of bedrock weathering on the chemical composition of the ice matrix without acidity. Factor 1 explains 40% of the variance in the upper and 36% in the lower lobe. Factor 2 revealed high loadings of H^+ and iron for both lobes, and additionally of cobalt, zinc and nickel for the upper lobe and aluminum for the lower lobe. Factor 2 is attributed to chemical weathering and the dissolution of metals driven by acidity as well as to atmospheric deposition. The explained variance was 30% in the upper and 26% in the lower lobe (Supplementary Table S2). The pattern of loadings on the two factors revealed a high similarity for most ions and metals in both lobes except for nickel (Supplementary Table S2; Figure 4). In the upper lobe, loading of nickel on factor 2 was very strong (0.98) and weak on factor 1 (0.06), while loadings on both factors in the lower lobe were similar (i.e. 0.52 vs. 0.69 for factor 1 and 2).

4 Discussion

4.1 Geochemical bedrock weathering

Geochemical weathering of bedrock minerals (i.e., paragneiss and micaschists of the Ötztal-Stubai Metamorphic Complex) has a major impact on the ion and metal concentrations found in the ice matrix of LZRG. Freeze-thaw weathering is widely discussed as a prominent agent of mechanical weathering in cold environments (Hall et al., 2002). The temporal availability of liquid water originating from rain events, snowmelt or internal ice-melt enables hydration and adsorption of water and water vapor on rock pore and crack surfaces. Wetting, drying and frost shattering of rocks is thus an effective combination for mechanical weathering in cold environments under water availability (Hall et al., 2002) creating eroded fractured rock surfaces. In addition, the downhill movement of the active rock glacier LZRG enhances the existence of freshly exposed mineral surfaces. Grain size tends to decrease with increasing depth and towards the front of the rock glacier, with fine-grained material more abundant in deepest layers, as was found for instance at LZRG (Krainer et al., 2015).

Intensified chemical weathering is expected to occur at the fractured rock faces (Williams et al., 2006) and, where liquid water is present, chemical weathering can be a major component of the overall weathering regime (Hall et al., 2002; Matsuoka and Murton, 2008). It is suggested that weathering in cold regions is not temperature limited, but rather the availability of moisture limits weathering (Hall et al., 2002; Williams et al., 2006). As moisture and liquid water within a rock glacier are available from rain events, snowmelt or internal ice-melt, we attribute a major fraction of ions and metals dissolved in the ice matrix of LZRG to mechanical and chemical weathering of bedrock minerals. The oxidation of pyrite and the related production of acidity intensify mineral weathering (Hall et al., 2002; Thies et al., 2007; Thies et al., 2013; Strauhal et al., 2016; Bucher et al., 2017).

Sulfide oxidation may occur through abiotic and biotic pathways and is controlled by factors like temperature, area of mineral surfaces, oxygen content and pH of the water, and it is mediated by microbial activity in this environment (Tranter et al., 2002;

Percak-Dennett et al., 2017). Sulfide oxidation may be coupled to carbonate and/or silicate weathering with carbonate weathering reactions being faster than silicate weathering (Tranter et al., 2002; Auqué et al., 2019). An indication on the preferred weathering pathway may be derived from the sulfate mass fraction (SMF = $SO_4^{2-}/(SO_4^{2-} + HCO_3^-)$). Values of SMF >0.5 point to sulfide oxidation coupled to silicate weathering assuming that other sulfate sources are small (Tranter et al., 2002). Ice from the LZRG core revealed SMF values >0.6 with a median SMF of 0.95 (Figure 5). In addition, dissolved ($Ca^{2+} + Mg^{2+}$) vs. SO_4^{2-} concentrations in the ice matrix were close to the 1:1 line (being highly correlated with $R^2 = 0.99$) (Figure 6). In view of stoichiometry of the related reactions (Tranter et al., 2002; Auqué et al., 2019) both SMF values and the molar ratio of (calcium + magnesium) vs. sulfate emphasize a prevalence of sulfuric acid silicate weathering at LZRG and fits to the available knowledge on the LZRG bedrock (Bressan, 2007; Krainer et al., 2015).

4.2 Atmospheric deposition and anthropogenic impact

In addition to geochemical weathering, prehistoric atmospheric deposition is a potential source of substances accumulated in the ice of LZRG. Mining and the related burning of biomass for copper metallurgy were likely sources of particulate and gaseous compounds to dry and wet atmospheric deposition in prehistoric times. Emission factors of the applied pyro-metallurgical methods were presumably high due to the uncontrolled mining and smelting procedures (Hong et al., 1996). Thus, emissions from firewood and particularly from metal ore mining and the smelting in open furnaces substantially contributed to the atmospheric deposition of metals like copper during the Antiquity (Hong et al., 1996). Rich copper deposits were mined in the Southeastern Alps during the Bronze Age sites of respective copper deposits and mines are indicated by Artioli et al. (2008); Lutz and Pernicka, (2013); Artioli et al. (2014); Artioli et al. (2016). From the Southeastern Alps, substantial copper production is reported from the second half of the 3rd millennium BC through the Recent Bronze Age, and copper sources presumably supplied most of Northern Italy (Artioli et al., 2016). An increased need for copper occurred with the introduction of coinage around 600 BC and a high copper production was reported during the Roman period (Hong et al., 1996).

Metals like nickel, arsenic, cobalt, zinc, and manganese were present at high concentrations of >1,000 ppm in many of the prehistoric alpine copper sulfide ores (Artioli et al., 2008). Besides, wood ash from biomass burning and charcoal use for metal ore production of copper (Pichler et al., 2013) can contain considerable amounts of metals like manganese, zinc, copper, and nickel (Narodoslawsky and Obernberger, 1996; Demeyer et al., 2001). Emissions of modern copper-nickel mining industries may serve as an indication of heavy metal release from ancient ore mining and smelting. For instance, high concentrations of heavy metals and sulfur are measured in precipitation, soil and surface waters at Kola Peninsula (Russia) and at Sudbury (Canada), reflecting the environmental pollution in the surrounding areas of copper-nickel industries (Hutchinson and Whitby, 1977; Dudka et al., 1995; Kashulina et al., 2014; Kashulina, 2017).

Distinct ice layers of the upper lobe of LZRG revealed peak concentrations of heavy metals (Figure 3). Apart from geochemical weathering, the high metal concentrations point to a certain anthropogenic impact of copper mining as a source of atmospheric trace substances that were dry and wet deposited and accumulated within the ice of LZRG. High values of copper and nickel in the uppermost LZRG ice core layers relate to the period of 2,600–2,200 cal·yr BP. They are considered to partly reflect atmospheric deposition impacts of mining during the Iron Age and the early Roman Empire when large quantities of bronze utensils were produced (Hong et al., 1996). Earlier peaks of nickel and copper fall into the period of ~3,200 and 3,550 cal·yr BP and similar peaks were dated for this period in the core of a peat bog in the close vicinity of LZRG (Hirnsperger, 2017). In the lower lobe of LZRG, i.e., prior to ~4,400 cal·yr BP (Krainer et al., 2015), concentrations of cobalt, copper, nickel and zinc were about one order of magnitude lower than in the uppermost peak of the period 2,600–2,200 cal·yr BP (Figures 3, 5). This points to the absence of a major anthropogenic impact through metal mining on the chemistry of LZRG ice during this early period and fits to the background concentrations of nickel and copper in the nearby peat bog (Hirnsperger, 2017).

4.3 Atmospheric deposition and prehistoric volcanic eruptions

Another potential source of substances analysed in the ice matrix of the LZRG core are large volcanic eruptions. They introduce huge amounts of gases and debris into the atmosphere. The injected material is distributed across vast areas or even globally. In Arctic and Antarctic ice cores, layers of tephra and elevated acid concentration (mainly as sulfate) are related to large eruptions and volcanic signatures are used as time markers and help to synchronize between different ice cores (Sigl et al., 2022).

We have checked for a distinct layer of the LZRG ice core whether the high amounts of acidity and metals could be related to a large volcanic eruption. This layer between 11.9 and 12.5 m depth was characterized by the lowest pH value of the entire LZRG core (pH of 4.15) accompanied by high values of sulfate, calcium, manganese, iron, aluminum, cobalt, copper, and nickel (Figure 3; Figure 7). According to the age-depth model, the layer corresponds to an age interval of about 3,500–3,550 cal·yr BP. Pronounced peaks of sulfur, cobalt, copper, and nickel were also reported from a layer of a core taken in a peat bog at about 600 m distance from Lazaun rock glacier. This specific layer was dated to 3,430 cal·yr BP (Hirnsperger, 2017). A potential source for the peak substance concentrations in both cores, i.e., in the LZRG ice core and in the Lazaun peat bog core, could be large volcanic eruptions and the associated atmospheric deposition of ejected gases and debris.

Recently, the eruption of Aniakchak II in Alaska could be dated to 1628 BCE by synchronizing polar ice core records from Greenland and the Antarctic (Cole-Dai et al., 2021; Pearson et al., 2022; Sigl et al., 2022). Aniakchak II is considered to have caused one of the largest Northern Hemisphere sulfur injections in the last 4,000 years. Total sulfur injection is calculated to 52 ±17 Tg·S, which clearly exceeds the Tambora injection of 34 ±7 Tg·S in 1815 CE (Pearson et al., 2022). Before, the

eruption of Thera on the Greek island of Santorini has long been discussed to have occurred in the 17th century BCE. Thera eruption was one of the most explosive in the Holocene with a volcanic explosivity index VEI 7, and has covered the Minoan settlement of Akrotiri with meters of deposited debris and tephra (Pearson et al., 2022). But recent evaluations of bipolar ice cores have shifted the date of the Thera eruption towards 1611 BCE, 1,562–1555 BCE or 1538 BCE, leaving the exact date still unconfirmed (McAneney and Baillie, 2019; Cole-Dai et al., 2021; Pearson et al., 2022).

In view of the uncertainties with the dating of the late Bronze Age Thera eruption, we may consider a time span of >100 years (1,628–1538 BCE) between the eruptions of Aniakchak II and Thera. This compares fairly well with the dated age of the above mentioned layer in the LZRG core (i.e. 3500–3,550 cal·yr BP) with high values of acidity, sulfate, calcium, manganese, iron, aluminum, cobalt, copper, and nickel. We therefore argue that the chemistry of this LZRG core layer reflects some impact of the large volcanic eruptions of Thera and Aniakchak II.

4.4 Chemical compounds in the ice of the LZRG core

We attributed the vertical profile of components dissolved in the ice of the LZRG core to a varying prevalence of both natural factors and human activities driving the chemical composition of the ice matrix through the past 10,000 years (Figure 7). To estimate the contribution of anthropogenic sources to the overall load of substances dissolved in the frozen LZRG core, we applied the crustal enrichment factor (EFc) method, which has been widely used in this context (Barbante et al., 2017; Spolaor et al., 2021). The crustal enrichment factor is defined as the ratio of a given element to a specific crustal tracer element, normalized to the concentration ratio of these elements in the upper continental crust (Barbante et al., 2017). As crustal tracer we used barium, and the element ratios in the Upper Continental Crust were taken from (Wedepohl, 1995). Values of EFs revealed a clear difference along the vertical core profile. In the lower lobe, mean EFs of the selected elements were 7 (copper), 10 (zinc), 22 (cobalt), 26 (nickel) and 50 (manganese). But mean values of EFs were by more than one order of magnitude higher in the upper lobe, except for manganese with an increase by a factor of <3 (Figure 7; Supplementary Figure S1). The high average EFs in the upper lobe support our interpretation that prehistoric anthropogenic sources added up to geochemical weathering, while in the lower lobe concentrations of ions and metals were mainly driven by the weathering of bedrock minerals.

In particular, the fine grained sediment layers in the lower part of the core are attributed to intense mechanical weathering and provide an enhanced reactive surface area for chemical weathering, which very likely caused the highest ion concentrations of the entire LZRG ice core. In the upper lobe, the oxidation of pyrite and the production of acidity enhanced chemical weathering. Sulfuric acid silicate weathering is considered to result in layers of acidic pH values and high concentrations of sulfate, base cations and metals (aluminum, cobalt, iron, nickel, zinc) prevailing in the upper lobe of the LZRG ice core. Anthropogenic impacts occurred *via* atmospheric deposition of gases and particles and were most likely limited to the last ~3,500 years. Prehistoric metal ore mining and the related burning of wood, that was necessary for smelting procedures and metal ore production of copper, were potential sources releasing considerable amounts of heavy metals to the atmosphere. Dry and wet deposition are expected to have contributed to the peak values of metals like copper or nickel in the upper lobe of the LZRG core thus potentially increasing the amount of substances derived from geochemical weathering (Figure 7). Large historic volcanic eruptions like those of Aniakchak II (Alaska) and Thera (Santorini, Greece) ejected high amounts of debris and gases (like sulfur) into the atmosphere and signals of tephra and elevated acid concentration were found in polar ice (Sigl et al., 2022). In the LZRG core, the layer dated to 3,500—3,550 cal·yr BP revealed high values of acidity, sulfate and metals like aluminum, copper or nickel. The large volcanic eruptions of Aniakchak II and Thera may thus have contributed to the high substance concentrations of this particular layer (Figure 7). In return, the high amount of acidity may have enhanced rates of geochemical weathering.

To summarize, geochemical weathering and atmospheric deposition of gases and particles from anthropogenic and natural sources (mining, biomass burning, large volcanic eruptions) were the driving factors of ion and metal concentrations in the ice of the LZRG core. The interpretation of two factors extracted from factor analysis discriminates processes related to acidity from those without acidity. Base cations, sulfate, silica, strontium and barium strongly loaded on the factor representing weathering without acidity, while aluminum, copper, iron and zinc strongly loaded on the factor related to the presence of acidity. The occurrence of nickel in the ice matrix of the LZRG core was related to acidity in the upper lobe. But we also found low amounts of nickel in the µg/L range (median nickel concentration of 7 µg/L) in the ice below 18 m depth, where pH values were above pH seven and accordingly aluminum concentrations were close to or below the limit of detection. This pattern was also reported for Lake Leit, a high mountain lake in the Swiss Alps, and its rock glacier impacted inflows (Steingruber et al., 2021). Nickel concentrations of these waters ranged between 6 and 18 µg/L, while nickel values <1 µg/L were given for streams not impacted by the rock glacier. We assume that nickel in the lower lobe of LZRG originated from the bedrock, and geochemical weathering may release small amounts of nickel. This is supported by the presence of nickel in paragneiss and orthogneiss samples of catchments in the Ötztal Alps (Krummgampen and Köfels, Austria) with a similar bedrock as in Lazaun, (i.e., Ötztal-Stubai metamorphic complex) (Purtscheller et al., 1995; Schönherr, 2009; Thies et al., 2018).

The uppermost 60 cm of the frozen LZRG core experienced periods of positive temperatures during summer months (Figure 2). We therefore assume that these layers of the LZRG core had already been exposed to partial contemporary melting and preferential elution of substances accumulated in the ice. Percolating precipitation and snow and ice melt are expected to be responsible for the reduction of substance concentrations in the top layers of the ice matrix (Figure 3). An increase in the active layer thickness was reported from permafrost sites across Europe, particularly from the European Alps with a pronounced thawing of the active layer in the warm summers of 2003 and 2015 (Etzelmüller et al., 2020). An increase in mountain permafrost temperatures of 0.19°C ± 0.05°C/decade (relative to 2008–2009) was given by Biskaborn et al. (2019) and a global analysis suggested a further permafrost warming under projected climate

scenarios with anthropogenic climate change as key driver of northern hemisphere permafrost warming (Gudmundsson et al., 2022; Smith et al., 2022). The degradation of ice below the active layer will reduce the water volume equivalent stored within the rock glacier causing both an increasing hydrological contribution and an export of solute-rich waters to downstream areas (Colombo et al., 2018a; Jones et al., 2019).

5 Conclusion

We present the chemical composition of the ice matrix of an active rock glacier in the Central Eastern Alps (Lazaun, Italy). The frozen core extended down to a depth of 28 m and covered an age of about 10,000 years. It consisted of two active lobes separated by an almost ice-free debris layer. Both lobes of the core had layers of high solute content with peak values of electrical conductivity >1,000 µS/cm. Sulfate, calcium and magnesium comprised ~90% of the dissolved ion load in the entire frozen core. The two lobes differed in acidity and metal concentrations—low pH and high levels of elements like cobalt, nickel, zinc, manganese, iron and aluminum prevailed in the upper lobe, while pH > 7 and low metal values were characteristic of the lower lobe. The concentrations of solutes are driven by geochemical weathering of bedrock minerals. Superimposed prehistoric atmospheric deposition from metal ore mining, wood (biomass) burning and large volcanic eruptions (Thera, Aniakchak II) may add up to increased substance loads in certain layers of the upper LZRG lobe.

Data availability statement

The raw data supporting the conclusion of this article will be made available by the authors, without undue reservation.

Author contributions

VM, KL, and DT designed, organized, and performed fieldwork. UN, HT, and KK sectioned and prepared the ice core for chemical analysis. UN and HT ran chemical ion analyses of ice core samples. UN and HT designed and wrote the paper with input from all co-authors.

Funding

This study was funded by PermaNet (Permafrost Long-term Monitoring Network, Interreg Alpine Space Project), and by the project Permaqua (Interreg IV Italy-Austria). We acknowledge financial support by the publishing fund of the University of Innsbruck and by the Faculty of Geo- and Atmospheric Sciences.

Acknowledgments

We especially appreciate our late colleague Richard Tessardi, who has performed metal analysis.

Conflict of interest

The authors declare that the research was conducted in the absence of any commercial or financial relationships that could be construed as a potential conflict of interest.

Publisher's note

Supplementary material

The Supplementary Material for this article can be found online at: https://www.frontiersin.org/articles/10.3389/feart.2023.1141379/full#supplementary-material

References

Arenson, L., Hoelzle, M., and Springman, S. (2002). Borehole deformation measurements and internal structure of some rock glaciers in Switzerland. *Permafr. Periglac. Process.* 13, 117–135. doi:10.1002/ppp.414

Artioli, G., Angelini, I., Nimis, P., Addis, A., and Villa, I. M. (2014). Prehistoric copper metallurgy in the Italian eastern Alps: Recent results. *Hist. Metall.* 47, 51–59.

Artioli, G., Angelini, I., Nimis, P., and Villa, I. M. (2016). A lead-isotope database of copper ores from the southeastern Alps: A tool for the investigation of prehistoric copper metallurgy. *J. Archaeol. Sci.* 75, 27–39. doi:10.1016/j.jas.2016.09.005

Artioli, G., Baumgarten, B., Marelli, M., Guissani, B., Recchia, S., Nimis, P., et al. (2008). Chemical and isotopic tracers in alpine copper deposits: Geochemical links between mines and metal. *Geo. Alp.*, 139–148.

Auqué, L. F., Puigdomenech, I., Tullborg, E.-L., Gimeno, M. J., Grodzinsky, K., and Hogmalm, K. J. (2019). Chemical weathering in a moraine at the ice sheet margin at Kangerlussuaq, Western Greenland. *Arct. Antarct. Alp. Res.* 51, 440–459. doi:10.1080/15230430.2019.1660125

Barbante, C., Spolaor, A., Cairns, W. R. L., and Boutron, C. (2017). Man's footprint on the Arctic environment as revealed by analysis of ice and snow. *Earth-Science Rev.* 168, 218–231. doi:10.1016/j.earscirev.2017.02.010

Barsch, D. (1996). *Rockglaciers: Indicators for the present and former geoecology in high mountain environments*. Berlin: Springer.

Barsch, D., Fierz, H., and Haeberli, W. (1979). Shallow core drilling and bore-hole measurements in the permafrost of an active rock glacier near the grubengletscher, wallis, Swiss Alps. *Arct. Alp. Res.* 11, 215–228. doi:10.2307/1550646

Biskaborn, B. K., Smith, S. L., Noetzli, J., Matthes, H., Vieira, G., Streletskiy, D. A., et al. (2019). Permafrost is warming at a global scale. *Nat. Commun.* 10, 264. doi:10.1038/s41467-018-08240-4

Bressan, D. (2007). *Aufbau und Dynamik aktiver Blockgletscher am Beispiel der Lazaunalm (Ötztaler Alpen/Südtirol)* (Innsbruck: University of Innsbruck, Department of Geology). Master thesis.

Brighenti, S., Tolotti, M., Bruno, M. C., Engel, M., Wharton, G., Cerasino, L., et al. (2019a). After the peak water: The increasing influence of rock glaciers on alpine river systems. *Hydrol. Process.* 33, 2804–2823. doi:10.1002/hyp.13533

Brighenti, S., Tolotti, M., Bruno, M. C., Wharton, G., Pusch, M. T., and Bertoldi, W. (2019b). Ecosystem shifts in alpine streams under glacier retreat and rock glacier thaw: A review. *Sci. Total Environ.* 675, 542–559. doi:10.1016/j.scitotenv.2019.04.221

Bucher, K., Zhou, W., and Stober, I. (2017). Rocks control the chemical composition of surface water from the high Alpine Zermatt area (Swiss Alps). *Swiss J. Geosciences* 110, 811–831. doi:10.1007/s00015-017-0279-y

Cole-Dai, J., Ferris, D. G., Kennedy, J. A., Sigl, M., McConnell, J. R., Fudge, T. J., et al. (2021). Comprehensive record of volcanic eruptions in the Holocene (11,000 years) from the WAIS divide, Antarctica ice core. *Geophys Res. Atmos.* 1, 126. doi:10.1029/2020JD032855

Colombo, N., Ferronato, C., Vittori Antisari, L., Marziali, L., Salerno, F., Fratianni, S., et al. (2020). A rock-glacier – pond system (NW Italian Alps): Soil and sediment properties, geochemistry, and trace-metal bioavailability. *CATENA* 194, 104700. doi:10.1016/j.catena.2020.104700

Colombo, N., Salerno, F., Gruber, S., Freppaz, M., Williams, M., Fratianni, S., et al. (2018a). Review: Impacts of permafrost degradation on inorganic chemistry of surface fresh water. *Glob. Planet. Change* 162, 69–83. doi:10.1016/j.gloplacha.2017.11.017

Colombo, N., Salerno, F., Martin, M., Malandrino, M., Giardino, M., Serra, E., et al. (2019). Influence of permafrost, rock and ice glaciers on chemistry of high-elevation ponds (NW Italian Alps). *Sci. Total Environ.* 685, 886–901. doi:10.1016/j.scitotenv.2019.06.233

Colombo, N., Sambuelli, L., Comina, C., Colombero, C., Giardino, M., Gruber, S., et al. (2018b). Mechanisms linking active rock glaciers and impounded surface water formation in high-mountain areas. *Earth Surf. Process. Landforms* 43, 417–431. doi:10.1002/esp.4257

Demeyer, A., Voundi Nkana, J., and Verloo, M. (2001). Characteristics of wood ash and influence on soil properties and nutrient uptake: An overview. *Bioresour. Technol.* 77, 287–295. doi:10.1016/s0960-8524(00)00043-2

Dudka, S., Ponce-Hernandez, R., and Hutchinson, T. C. (1995). Current level of total element concentrations in the surface layer of Sudbury's soils. *Sci. Total Environ.* 162, 161–171. doi:10.1016/0048-9697(95)04447-9

Etzelmüller, B., Guglielmin, M., Hauck, C., Hilbich, C., Hoelzle, M., Isaksen, K., et al. (2020). Twenty years of European mountain permafrost dynamics—The PACE legacy. *Environ. Res. Lett.* 15, 104070. doi:10.1088/1748-9326/abae9d

Fegel, T. S., Baron, J. S., Fountain, A. G., Johnson, G. F., and Hall, E. K. (2016). The differing biogeochemical and microbial signatures of glaciers and rock glaciers. *J. Geophys. Res. Biogeosci.* 121, 919–932. doi:10.1002/2015jg003236

Gudmundsson, L., Kirchner, J., Gädeke, A., Noetzli, J., and Biskaborn, B. K. (2022). Attributing observed permafrost warming in the northern hemisphere to anthropogenic climate change. *Environ. Res. Lett.* 17, 095014. doi:10.1088/1748-9326/ac8ec2

Guglielmin, M., Camusso, M., Polesello, S., and Valsecchi, S. (2004). An old relict glacier body preserved in permafrost environment: The Foscagno rock glacier ice core (upper valtellina, Italian central Alps). *Arct. Antarct. Alp. Res.* 36, 108–116. doi:10.1657/1523-0430(2004)036[0108:aorgbp]2.0.co;2

Haeberli, W. (1985). Creep of mountain permafrost: Internal structure and flow of alpine rock glaciers. *Mittl. Vers. für Wasserbau, Hydrol. Glaziologie, ETH Zurich* 77, 5–142.

Haeberli, W., Hallet, B., Arenson, L., Elconin, R., Humlum, O., Kääb, A., et al. (2006). Permafrost creep and rock glacier dynamics. *Permafr. Periglac. Process.* 17, 189–214. doi:10.1002/ppp.561

Haeberli, W., Hoelzle, M., Kääb, A., Keller, F., and Wagner, S. (1998). Ten years after drilling the permafrost of the active rock glacier Murtel, eastern Swiss Alps: Answered questions and new perspectives. *Proc. 7th Int. Permafr. Conf. Yellowknife (Canada), Collect. Nordicana* 55, 403–410.

Haeberli, W., Kääb, A., Wagner, S., Mühll, D. V., Geissler, P., Haas, J. N., et al. (1999). Pollen analysis and 14C age of moss remains in a permafrost core recovered from the active rock glacier murtèl-corvatsch, Swiss Alps: Geomorphological and glaciological implications. *J. Glaciol.* 45, 1–8. doi:10.3189/s0022143000002975

Hall, K., Thorn, C. E., Matsuoka, N., and Prick, A. (2002). Weathering in cold regions: Some thoughts and perspectives. *Prog. Phys. Geogr. Earth Environ.* 26, 577–603. doi:10.1191/0309133302pp353ra

Hauck, C., Böttcher, M., and Maurer, H. (2011). A new model for estimating subsurface ice content based on combined electrical and seismic data sets. *Cryosphere* 5, 453–468. doi:10.5194/tc-5-453-2011

Hausmann, H., Krainer, K., Brückl, E., and Mostler, W. (2007). Internal structure and ice content of Reichenkar rock glacier (Stubai Alps, Austria) assessed by geophysical investigations. *Permafr. Periglac. Process.* 18, 351–367. doi:10.1002/ppp.601

Hausmann, H., Krainer, K., Brückl, E., and Ullrich, C. (2012). Internal structure, ice content and dynamics of Ölgrube and Kaiserberg rock glaciers (Ötztal Alps, Austria) determined from geophysical surveys. *Austrian J. Earth Sci.* 105, 12–31.

Hirnsperger, M. (2017). *Die quartären Sedimente im Bereich der Lazaun Alm, südliche Ötztaler Alpen (Südtirol)* (Innsbruck: University of Innsbruck, Department of Geology). Master thesis.

Hoinkes, G., Krainer, K., and Tropper, P. (2021). Ötztaler Alpen, Stubaier Alpen und Texelgruppe. *Sammlung Geologischer Führer*.

Hoinkes, G., and Thöni, M. (1993). "Evolution of the Ötztal-Stubai, Scarl-Campo and Ulten Basement Units," in. *Pre-Mesozoic Geology in the Alps*. Editors J. F. von Raumer and F. Neubauer (Berlin, Heidelberg: Springer Berlin Heidelberg), 485–494. doi:10.1007/978-3-642-84640-3_29

Hong, S., Candelone, J.-P., Soutif, M., and Boutron, C. F. (1996). A reconstruction of changes in copper production and copper emissions to the atmosphere during the past 7000 years. *Sci. Total Environ.* 188, 183–193. doi:10.1016/0048-9697(96)05171-6

Hutchinson, T. C., and Whitby, L. M. (1977). The effects of acid rainfall and heavy metal particulates on a boreal forest ecosystem near the Sudbury smelting region of Canada. *Water, Air, Soil Pollut.* 7, 421–438. doi:10.1007/bf00285542

Ilyashuk, B. P., Ilyashuk, E. A., Psenner, R., Tessadri, R., and Koinig, K. A. (2014). Rock glacier outflows may adversely affect lakes: Lessons from the past and present of two neighboring water bodies in a crystalline-rock watershed. *Environ. Sci. Technol.* 48, 6192–6200. doi:10.1021/es500180c

Jones, D. B., Harrison, S., Anderson, K., and Whalley, W. B. (2019). Rock glaciers and mountain hydrology: A review. *Earth-Science Rev.* 193, 66–90. doi:10.1016/j.earscirev.2019.04.001

Kashulina, G., Caritat, P., and Reimann, C. (2014). Snow and rain chemistry around the "Severonikel" industrial complex, NW Russia: Current status and retrospective analysis. *Atmos. Environ.* 89, 672–682. doi:10.1016/j.atmosenv.2014.03.008

Kashulina, G. M. (2017). Extreme pollution of soils by emissions of the copper–nickel industrial complex in the Kola Peninsula. *Eurasian Soil Sc.* 50, 837–849. doi:10.1134/s1064229317070031

Krainer, K., Bressan, D., Dietre, B., Haas, J. N., Hajdas, I., Lang, K., et al. (2015). A 10,300-year-old permafrost core from the active rock glacier Lazaun, southern Ötztal Alps (South Tyrol, northern Italy). *Quat. Res.* 83, 324–335. doi:10.1016/j.yqres.2014.12.005

Leopold, M., Williams, M. W., Caine, N., Völkel, J., and Dethier, D. (2011). Internal structure of the green lake 5 rock glacier, Colorado front range, USA. *Permafr. Periglac. Process.* 22, 107–119. doi:10.1002/ppp.706

Lutz, J., and Pernicka, E. (2013). Prehistoric copper from the eastern Alps. *Open J. Archaeom.* 1, 25. doi:10.4081/arc.2013.e25

Matsuoka, N., and Murton, J. (2008). Frost weathering: Recent advances and future directions. *Permafr. Periglac. Process.* 19, 195–210. doi:10.1002/ppp.620

McAneney, J., and Baillie, M. (2019). Absolute tree-ring dates for the Late Bronze Age eruptions of Aniakchak and Thera in light of a proposed revision of ice-core chronologies. *Antiquity* 93, 99–112. doi:10.15184/aqy.2018.165

Narodoslawsky, M., and Obernberger, I. (1996). From waste to raw material-the route from biomass to wood ash for cadmium and other heavy metals. *J. Hazard. Mater.* 50, 157–168. doi:10.1016/0304-3894(96)01785-2

Pearson, C., Sigl, M., Burke, A., Davies, S., Kurbatov, A., Severi, M., et al. (2022). Geochemical ice-core constraints on the timing and climatic impact of Aniakchak II (1628 BCE) and Thera (Minoan) volcanic eruptions. *PNAS Nexus* 1, 1. doi:10.1093/pnasnexus/pgac048

Percak-Dennett, E., He, S., Converse, B., Konishi, H., Xu, H., Corcoran, A., et al. (2017). Microbial acceleration of aerobic pyrite oxidation at circumneutral pH. *Geobiology* 15, 690–703. doi:10.1111/gbi.12241

Peszek, Ł., Kawecka, B., and Robinson, C. T. (2022). Long-term response of diatoms in high-elevation streams influenced by rock glaciers. *Ecol. Indic.* 144, 109515. doi:10.1016/j.ecolind.2022.109515

Pichler, T., Nicolussi, K., Goldenberg, G., Hanke, K., Kovács, K., and Thurner, A. (2013). Charcoal from a prehistoric copper mine in the Austrian Alps: Dendrochronological and dendrological data, demand for wood and forest utilisation. *J. Archaeol. Sci.* 40, 992–1002. doi:10.1016/j.jas.2012.09.008

Purtscheller, F., Pirchl, T., Sieder, G., Stingl, V., Tessadri, T., Brunner, P., et al. (1995). Radon emanation from giant landslides of koefels (tyrol, Austria) and langtang himal (Nepal). *Geo* 26, 32–38. doi:10.1007/bf00776029

Schönherr, M. (2009). *Bachelor thesis*. Innsbruck: University of Innsbruck, Department of Geology.

Sigl, M., Toohey, M., McConnell, J. R., Cole-Dai, J., and Severi, M. (2022). Volcanic stratospheric sulfur injections and aerosol optical depth during the Holocene (past 11 500 years) from a bipolar ice-core array. *Earth Syst. Sci. Data* 14, 3167–3196. doi:10.5194/essd-14-3167-2022

Smith, S. L., O'Neill, H. B., Isaksen, K., Noetzli, J., and Romanovsky, V. E. (2022). The changing thermal state of permafrost. *Nat. Rev. Earth Environ.* 3, 10–23. doi:10.1038/s43017-021-00240-1

Spolaor, A., Moroni, B., Luks, B., Nawrot, A., Roman, M., Larose, C., et al. (2021). Investigation on the sources and impact of trace elements in the annual snowpack and the firn in the hansbreen (southwest spitsbergen). *Front. Earth Sci.* 8, 1. doi:10.3389/feart.2020.536036

Steig, E. J., Fitzpatrick, J. J., Potter, jr., N., and Clark, D. H. (1998). The geochemical record in rock glaciers. *Geogr. Ann. Ser. A, Phys. Geogr.* 80, 277–286. doi:10.1111/j.0435-3676.1998.00043.x,

Steingruber, S. M., Bernasconi, S. M., and Valenti, G. (2021). Climate change-induced changes in the chemistry of a high-altitude mountain lake in the central Alps. *Aquat. Geochem* 27, 105–126. doi:10.1007/s10498-020-09388-6

Strauhal, T., Prager, C., Millen, B., Spötl, C., Zangerl, C., and Brandner, R. (2016). Aquifer geochemistry of crystalline rocks and Quaternary deposits in a high altitude alpine environment (Kauner Valley, Austria). *AJES 109* 109. doi:10.17738/ajes.2016.0002

Thies, H., Nickus, U., Mair, V., Tessadri, R., Tait, D., Thaler, B., et al. (2007). Unexpected response of high Alpine Lake waters to climate warming. *Environ. Sci. Technol.* 41, 7424–7429. doi:10.1021/es0708060

Thies, H., Nickus, U., Tessadri, R., Tropper, P., and Krainer, K. (2018). Peculiar arsenic, copper, nickel, uranium, and yttrium-rich stone coatings in a high mountain stream in the Austrian Alps. *AJES* 110, 1. doi:10.17738/ajes.2017.0012

Thies, H., Nickus, U., Tolotti, M., Tessadri, R., and Krainer, K. (2013). Evidence of rock glacier melt impacts on water chemistry and diatoms in high mountain streams. *Cold Regions Sci. Technol.* 96, 77–85. doi:10.1016/j.coldregions.2013.06.006

Tranter, M., Sharp, M. J., Lamb, H. R., Brown, G. H., Hubbard, B. P., and Willis, I. C. (2002). Geochemical weathering at the bed of Haut Glacier d'Arolla, Switzerland?a new model. *Hydrol. Process.* 16, 959–993. doi:10.1002/hyp.309

Wedepohl, K. H. (1995). The composition of the continental crust. *Geochimica et Cosmochimica Acta*. 59, 1217–1232. doi:10.1016/0016-7037(95)00038-2

Williams, M. W., Knauf, M., Caine, N., Liu, F., and Verplanck, P. L. (2006). Geochemistry and source waters of rock glacier outflow, Colorado Front Range. *Permafr. Periglac. Process.* 17, 13–33. doi:10.1002/ppp.535

Williams, M. W., Knauf, M., Cory, R., Caine, N., and Liu, F. (2007). Nitrate content and potential microbial signature of rock glacier outflow, Colorado Front Range. *Earth Surf. Process. Landforms* 32, 1032–1047. doi:10.1002/esp.1455